Title: Molecular dynamics and cold crystallization process in a liquid-crystalline substance with para-, ferro- and antiferro-electric phases as studied by dielectric spectroscopy and scanning calorimetry

Author: Łukasz Kolek, Maria Massalska-Arodź, Karolina Adrjanowicz, Tomasz Rozwadowski, Kamil Dychtoń, Marcin Drajewicz i in.

Citation style: Kolek Łukasz, Massalska-Arodź Maria, Adrjanowicz Karolina, Rozwadowski Tomasz, Dychtoń Kamil, Drajewicz Marcin i in. (2020). Molecular dynamics and cold crystallization process in a liquid-crystalline substance with para-, ferro- and antiferro-electric phases as studied by dielectric spectroscopy and scanning calorimetry. “Journal of Molecular Liquids” (Vol. 297 (2020), Art. No. 111913), doi 10.1016/j.molliq.2019.111913

Journal of Molecular Liquids 297 (2020) 111913

Contents lists available at ScienceDirect

Journal of Molecular Liquids

journal homepage: www.elsevier.com/locate/molliq

Molecular dynamics and cold crystallization process in a liquid-crystalline substance with para-, ferro- and antiferro-electric phases as studied by dielectric spectroscopy and scanning calorimetry

Łukasz Kolek [a,*], Maria Massalska-Arodź [b], Karolina Adrjanowicz [c], Tomasz Rozwadowski [b,d], Kamil Dychtoń [a], Marcin Drajewicz [a], Przemysław Kula [e]

[a] Department of Material Science, Rzeszow University of Technology, Rzeszów, Poland
[b] Institute of Nuclear Physics, Polish Academy of Sciences, Kraków, Poland
[c] Department of Biophysics and Molecular Physics, Institute of Physics, University of Silesia, Chorzów, Poland
[d] Department of Chemistry, Faculty of Pure and Applied Sciences, University of Tsukuba, Tsukuba, Ibaraki, 305-8571, Japan
[e] Institute of Chemistry, Military University of Technology, Warsaw, Poland

ARTICLE INFO

Article history:
Received 8 June 2019
Received in revised form 28 September 2019
Accepted 11 October 2019
Available online 17 October 2019

Keywords:
Liquid crystal
Dielectric spectroscopy
Differential scanning calorimetry
Cold crystallization

ABSTRACT

In this article, molecular dynamics and the cold crystallization kinetics of 4-(6-heptafluorobutanoiloxyhexyloxy) biphenyl-4′-carboxylan(S)-4-(1-methyloheptyloxycarbonyl) phenyl (abbreviated as 3F6Bi and/or 4H6) are presented. Rich polymorphism of the liquid-crystalline (SmA*, SmC*, SmC^*_A and SmI^*_A) phases and partially disordered crystal CrI and glassy GCrI were observed upon cooling. Both, molecular and collective relaxation processes were observed in the para-, ferro- and antiferro-electric liquid-crystalline phases over the frequency range of 3×10^{-2} to 3×10^{6} Hz. An additional bias field in the dielectric experiments was used to identify individual processes. The high heating rates (5–10 K/min) phase sequence is the same as in case of the cooling experiment. On slow heating (0.5–2 K/min), cold crystallization of SmI^*_A to the more stable crystal CrII phase was observed in the dielectric and calorimetric experiments. The crystallization kinetics was analyzed using the Mo equation, which is a combination of the Avrami and Ozawa models. The activation energy of crystallization was calculated to be 138 and 99 kJ/mol using the Kissinger and Augis-Bennett models, respectively.

1. Introduction

Antiferroelectric liquid-crystalline substances having three phenyl rings in their molecular core are intensively studied as components of mixtures for next generation liquid crystal displays [1–3]. These substances have usually rich phase polymorphism containing liquid crystalline, glassy, and metastable or stable crystalline phases [4,5]. Most of high-temperature liquid-crystalline phases in these substances are enantiotropic, while at low temperatures the phase sequence often depends on the rate of temperature changes. On heating, metastable phases (solid or liquid-crystalline) transform to give stable crystals through the cold crystallization processes [6,7]. Studies of 4-(6-heptafluorobutanoiloxy hexyloxy)biphenyl-4′-carboxylan(S)-4-(1-methyloheptyloxycarbonyl)phenyl's (abbreviated as 3F6Bi) cold crystallization kinetics by differential scanning calorimetry (DSC) and dielectric spectroscopy methods are one of the purposes of this paper. The main aim of this work is to confirm the phase sequence for 3F6Bi, to investigate the influence of the heating rate on phase transitions, and to identify and describe the molecular dynamics of the liquid-crystalline phases using broadband dielectric spectroscopy, with bias electric field applied. A schematic of the molecular structure of 3F6Bi, calculated using the PM6 method, is shown in Fig. 1.

The central core of the 3F6Bi molecule, synthesized at the Institute of Chemistry, Military University of Technology, Warsaw, is based on phenyl biphenylate unit (biphenyl ring connected with phenyl ring via COO- group). Such superposition of rings in the core unit is known for stabilizing the anticlinic arrangement [8,9]. The core unit is connected with an achiral perfluoroalkanoiloxy chain by a hexyloxy spacing chain on the biphenyl moiety. These connections facilitate a low melting point and the SmA*-SmC*-SmC^*_A sequence. The phenyl side of the core is connected to the chiral chain by an ester linkage. The chiral center is derived from (S)-2-octanol. Values of the components of dipole molecular moments are given in Fig. 1.

The 3F6Bi substance has been previously studied by differential scanning calorimetry (DSC), transmission light intensity method (TLI),

* Corresponding author.
E-mail address: kolek@prz.edu.pl (Ł Kolek).

https://doi.org/10.1016/j.molliq.2019.111913

a)

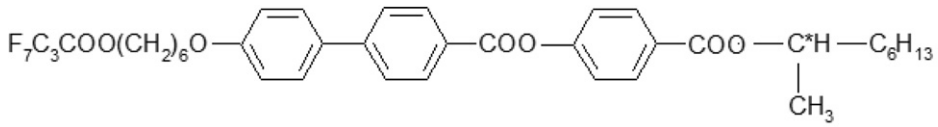

b)

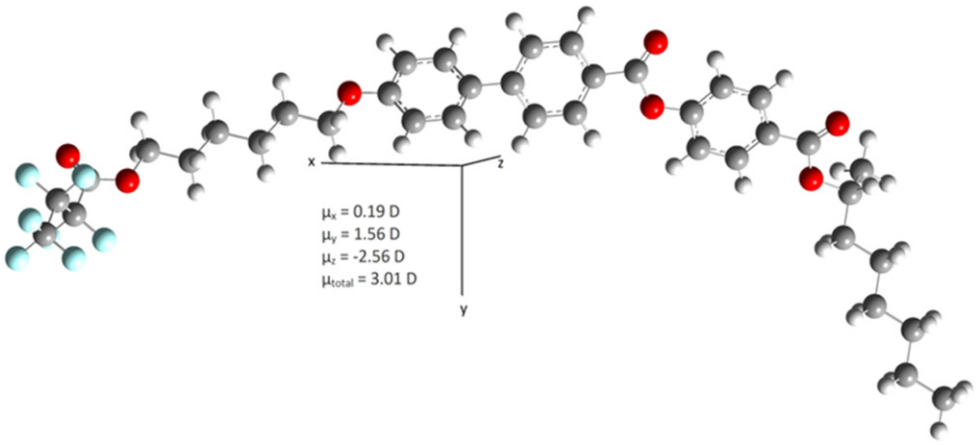

Fig. 1. The molecular structure of 4-(6-heptafluorobutanoiloxy hexyloxy)biphenyl-4′-carboxylan(S)-4-(1-methyloheptyloxycarbonyl)phenyl (3F6Bi): chemical formula (a) and structure calculated using the PM6 method (b). The values of components of molecular dipole moment are given.

and polarizing microscopy observations (POM) [10,11]. The results from these methods, as well as results from dielectric spectroscopy experiments (described in this paper), allow one to determine, for 3F6Bi, the following phase sequence on cooling:

Is (129 °C) SmA* (122 °C) SmC* (111 °C) SmC^*_A (6 °C) SmI^*_A (−24 °C) CrI (~-90 °C) GCrI.

Long-range order of some degrees of freedom present in the CrI phase is frozen-in during the vitrification process. The phase sequence on heating strongly depends on the rate of temperature changes and is discussed in the paper.

2. Experimental

Dielectric spectra $\varepsilon^*(\nu,T) = \varepsilon'(\nu,T) - i\varepsilon''(\nu,T)$ of 3F6Bi were obtained using a Novocontrol Alpha dielectric spectrometer at the Institute of Physics, University of Silesia. All measurements were performed on non-oriented samples over a frequency range from 3×10^{-2} to 3×10^{6} Hz within the temperature region of −130 °C and 130 °C. The temperature was stabilized with an accuracy 0.2 K by a Quattro System temperature controller with a nitrogen gas cryostat. Before the measurement, the sample was heated above the clearing point temperature and put between brass disc electrodes with a 10 mm diameter. The thickness of the sample layer was 0.07 mm. Dielectric measurements started at 130 °C while the sample was cooled. Over temperature ranges from 130 °C to 100 °C and from 20 °C to −40 °C the dielectric spectra were collected every 2 °C, while from 100 °C to 20 °C and from −40 °C to −130 °C, 4 °C increments were used. Then, the substance was heated in the same regimes. The averaged time of measurement of the electric permittivity at each temperature was of approximately 20 min. Every measurement was repeated with the addition of a bias voltage of 2, 5, 10, 20, and 40 V. A complementary series of dielectric measurements were carried out at Henryk Niewodniczanski Institute of Nuclear Physics using the same type of spectrometer. This series was performed at a single frequency of 7×10^3 Hz, over the temperature range of −100 °C–140 °C on cooling and heating with various cooling/heating rates: 0.5, 1, 2, 5 and 10 K/min.

Texture observations were performed using a polarizing microscope (Opta-Tech) equipped with Linkam heating stage and temperature controller. Liquid nitrogen was used as a coolant. The polarizing microscope was equipped with a camera connected to the computer. Observations were performed during cooling over the temperature range of 140 °C to −150 °C for various rates.

Calorimetric analysis of cold crystallization kinetics were performed based on results from the Netsch differential scanning calorimeter. DSC thermograms were recorded for several cooling/heating rates: 0.5, 1, 2, 5 and 10 K/min over the temperature range of −70 °C–140 °C.

3. Results and discussion

3.1. Dynamics of the ferro- and antiferro-electric phases of 3F6Bi

In the dielectric measurements for the 3F6Bi dynamics was found in all liquid crystalline phases and in the partially disordered CrI and its glass. Fig. 2a, b, c, d shows the dielectric absorption as a function of frequency for the particular phases detected on slow cooling. In the paraelectric SmA* phase, a single, high-frequency relaxation process is observed. The spectrum recorded at the ferroelectric SmC* phase clearly reveals the presence of only one process at a frequency of approximately 10^2 Hz. Its intensity ($\varepsilon''_{max} \sim 600$) is much larger than that registered for process in SmA* phase, and completely dominates the dielectric spectrum, therefore one can suspect that other dynamic processes may be hidden in this region. One can see that in the antiferroelectric SmC^*_A and SmI^*_A phases (Fig. 2b and c), three relaxation processes are evident. The limited range of the measuring frequency means that not all of them can be observed over the whole temperature range in the SmC^*_A phase. In SmI^*_A all three processes were observed in the full temperature range of this phase. The intensity of every process in the antiferroelectric phases is comparable to the intensity of the process identified in SmA* phase and is much smaller than the intensity of the intensive process in the SmC* phase (Fig. 2a). In Fig. 2d a weak relaxation in CrI and a secondary relaxation in the glass of CrI is shown. Vitrification temperature $T_g \approx -90$ °C was estimated from a polarizing microscopy observation.

The dielectric spectra were analyzed using the Havriliak – Negami equation:

$$\varepsilon^*(\omega) = \varepsilon_\infty + \sum_i = 1^3 \frac{\Delta\varepsilon_i}{\left(1 + (i\omega\tau_i HN)_i^{1-\alpha}\right)_i^{\beta}} + \frac{A(\omega)}{\omega} \quad (1)$$

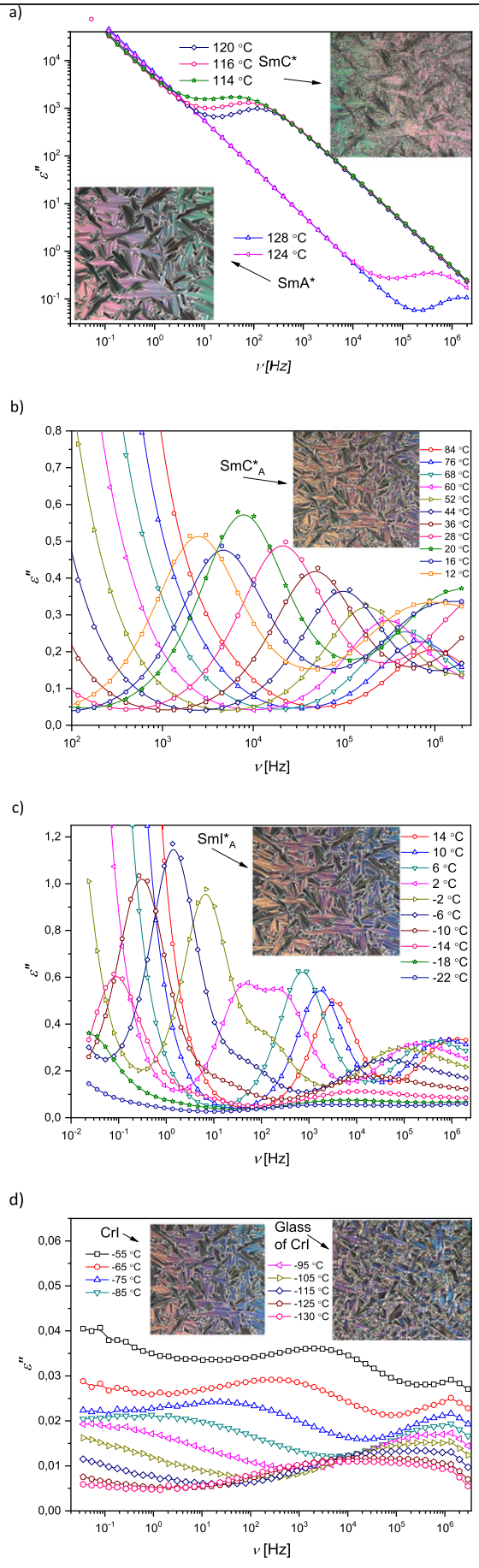

Fig. 2. The dielectric absorption as a function of frequency observed during slow cooling in the SmA* (128 and 124 °C) and ferroelectric SmC* (120–114 °C) (a), in the antiferroelectric SmC^*_A (84–12 °C), (b) in the antiferroelectric SmI^*_A (2 to −14 °C), (c) in partially disordered crystal CrI (−55 to −85 °C), and in glass GCrI (−95 to −130 °C) (d). Insets show the textures of particular phases. Cracking related to vitrification is shown in the texture of GCrI [10].

where $\Delta\varepsilon = \varepsilon_\infty - \varepsilon_0$, ε_∞ and ε_0 are low and high-frequency limit of electric permittivity, τ_H N is the macroscopic relaxation time, A/ω describes the ionic conductivity, and α and β are Havriliak-Negami shape parameters (α=0 and $\beta = 1$ correspond to the Debye process), $i = 1, 2, 3$ for first, second and third relaxation process, respectively. Fitting of Eq. (1) to the dielectric data allows one to find the contribution of the relaxation processes in the $\varepsilon''(\nu)$ spectra for each temperature. In Fig. 3, an example of the fitting results in the SmC^*_A phase are shown together with the relaxation time and the α and β shape parameters for the two identified relaxation processes. In order to differentiate the relaxation processes in the subsequent phases, the temperature dependence of the relaxation time and the temperature dependence of ε''_{max} for each process were calculated using Eq. (1) and presented in Fig. 4 and in Fig. 5, respectively.

Arrhenius plots (Fig. 6) enables the calculations of the energy barriers for subsequent processes found. For better identification of the mechanism of molecular dynamics in smectic phases of 3F6Bi, dielectric measurements were repeated with a bias field, *i.e.* in the presence of an additional electric field, which causes unwinding of the ferro- and antiferro-electric helices in the smectic phases. Then, relaxation processes connected with rotation of molecule around the cone by changing the azimuthal angle, *i.e.* Goldstone mode (GM) in the ferroelectric phase and phasons in the antiferroelectric phase, are frozen. This field also reduces the contribution from ionic conductivity and from that, it is possible to observe relaxation processes not -visible using standard measurements (Fig. 7 a, b, c).

Fitting the Havriliak-Negami formula to the obtained dielectric spectra shows that only two relaxation processes in the liquid crystal phases of 3F6Bi are sensitive to the bias field, *i.e.* the relaxation process in the ferroelectric SmC* phase (Fig. 7a) and low-frequency process (AFM5) in SmI^*_A phase (Fig. 7c). The relaxation process in SmA* phase is insensitive to the bias field and it has non-Arrhenius character. The values of the shape parameters ($\alpha = 0, \beta = 1$) correspond to the Debye process, which makes it clear that it is a soft mode (SM). In the SmC* phase of 3F6Bi, a decrease in the absorption intensity with increasing voltage of the bias field was observed. This, as well as its other features allow us to unambiguously identify this process as a Goldstone mode (GM). Non-Debye values of the shape parameters of this process (α ~ 0.3) suggest that another relaxation process with a smaller magnitude may be hidden in the $\varepsilon''(\nu)$ spectrum. This hypothesis has been confirmed in measurements with a bias field, as due to stretching of the helix, the Goldstone mode is frozen and in the spectrum one can observe the high-frequency soft mode (Fig. 7a). Both processes in the para- and ferro-electric phases have a non-Arrhenius character.

In the antiferroelectric phase, the theory predicts four possible collective processes (2 phasons and 2 amplitudons) and 2 molecular processes (l-process related to molecular reorientations around a long molecular axis and an s-process around a short axis). As shown in Fig. 4, in the SmC^*_A phase three peaks are observed (called AFM1, AFM2 and AFM3). Defining the individual processes found is usually complicated. Most of the authors of publications on dynamics in antiferroelectric phases have observed two relaxation processes in the SmC^*_A phase and their interpretation varies. Uchiyama et al. interpret them as an amplitudon and molecular s-process [12], however there are suggestions that both of them are collective processes [13,14]. None of the processes detected in SmC^*_A phase of 3F6Bi appear to be sensitive to the bias field, therefore we can conclude that they are not attributed to a phason. The lowest frequency process (AFM1) appears in dielectric spectrum just below the SmC^*-SmC^*_A transition. The values of the shape parameters ($\alpha = 0, \beta = 1$) are typical for the Debye process. The AFM1 relaxation is of Arrhenius type with an activation energy equal to 111 kJ/mol. The second relaxation process (AFM2) observed below 100 °C is Debye type and its intensity increases with decreasing temperature. The relaxation time of AFM2 process strongly depends on temperature in a non-Arrhenius way. The fastest process (AFM3) in SmC^*_A phase appears over a measurement frequency range available below 20 °C. The mode is temperature-dependent and possess Arrhenius character with 55 kJ/mol energy activation and its intensity lowers progressively upon cooling. Based on this information one can suspect that AFM1 and AFM3 are molecular processes related to reorientations around both short (s-process) and long (l-process) axes and the non-Arrhenius AFM2 process seems to be amplitudon. The same interpretation of the corresponding processes was concluded by Panarin et al. [15]. Continuation of the AFM3 process was observed in the SmI^*_A phase, so one can suspect that it is an l-process. The fastest of three observed processes registered in the SmI^*_A phase is interpreted similarly by Kolek et al. for 1F7 [16], whose molecules have many similarities to that of 3F6Bi. Both 1F7 and 3F6Bi molecules have the same chiral chain and for both, the second terminal chain has a C_3F_7 group. The molecules for both compounds have a biphenyl ring connected to the phenyl ring in the main core (via $(CH_2)_2$ in 1F7 and COO in 3F6Bi). In the phenyl core of 1F7, one F atom substitutes a H atom. As mentioned above, the AFM5 process in SmI^*_A of 3F6Bi is sensitive to a bias field, hence, one can deduce, that it is a ferroelectric phason. Based on the dependences of relaxation time and the ε_{max} in a function of temperature, presented in Figs. 4 and Fig. 5, one can observe that the AFM4 process is a continuation of the AFM2 process in the phase SmC^*_A, thus it is interpreted as a ferroelectric amplitudon. As one can see in

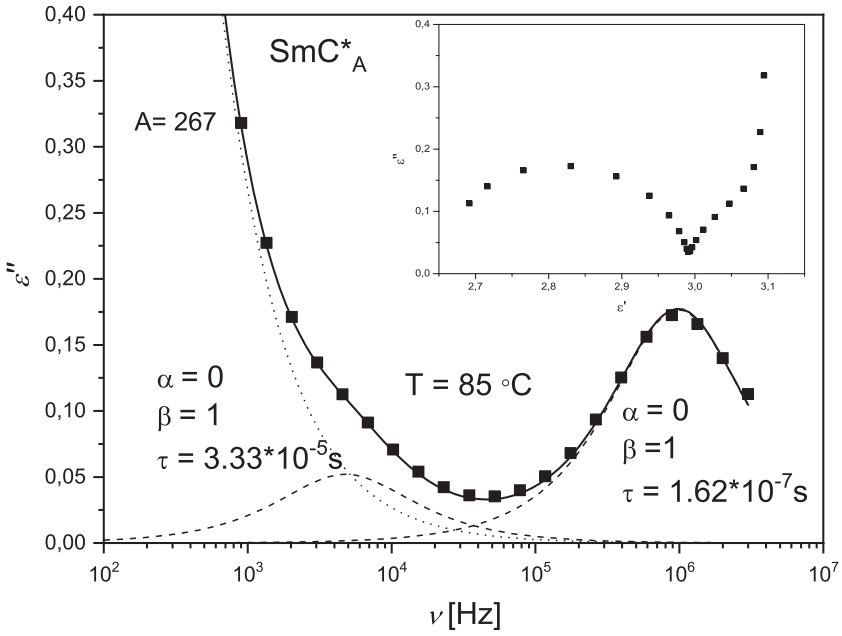

Fig. 3. The dielectric absorption as a function of frequency measured at 85 °C for the SmC^*_A phase of 3F6Bi. The solid line corresponds to the results of fitting Equation (1) to the experimental points. Dotted and dashed lines show the contribution of the electric conductivity and the two processes of dielectric relaxation. Inset shows the Cole–Cole plot at this temperature.

Fig. 6, the temperature dependence of the AFM2 relaxation time fulfills the Vogel-Fulcher-Tammann equation, while the AFM4 process is Arrhenius type. The AFM3 process is also observed over a temperature range 10 °C below the temperature of the CrI crystallization, but its intensity decreases rapidly as the temperature decreases. In CrI phase, weak non-Debye relaxation of the Arrhenius character with an activation energy of 95 kJ/mol was registered and ascribed to intramolecular motions of the terminal chains of molecules. The values of α parameter are of about 0.7 and β of about 0.8. Below vitrification, the faster secondary β-relaxation of activation energy equal to 33 kJ/mol was found. In the glass of CrI the shape parameters (α~0.5 and β~0.4) strongly deviate from Debye type relaxation which points to strong correlations of dynamics in local and long-range scales. Long-range correlations of cooperative motions in CrI are not so large.

Cold crystallization of CrII from the metastable SmI^*_A phase.

All experimental methods used show that on cooling 3F6Bi the antiferroelectric phase SmI^*_A transforms into a disordered crystal CrI phase, which is vitrified in the vicinity of −90 °C (based on polarizing microscopy observations). As seen in Fig. 8, the phase sequence registered by the DSC method is independent of cooling rate, exhibiting an isotropic liquid, four liquid crystalline phases, and CrI. The phase sequence observed on heating is more complicated. First, softening of the glassy GCrI phase to CrI and a transition to the SmI^*_A phase are observed. During further heating of the sample there are two scenarios: on slow heating (0.5, 1 and 2 K/min) cold crystallization of a new CrII and then transition to SmC^*_A occur, whilst in the case of higher heating rates (5 and 10 K/min) SmI^*_A does not crystallize and it transforms directly to the SmC^*_A phase. One can conclude that for fast heating, the phase sequence of 3F6Bi is enantiotropic while for slow heating an additional monotropic phase of more stable crystal CrII appears (see Fig. 9). Confirmation of these observations can be found in the dielectric experiments. Fig. 10 shows the dielectric dispersion at the selected 7×10^3 Hz frequency. When the temperature changes are slow (Fig. 10a) significant differences are visible in the $\varepsilon'(T)$ curves recorded during cooling and heating. In contrast, for higher rates of temperature changes the curves recorded on cooling and heating have almost the same shapes (Fig. 10b), this confirms the enantiotropic character of the phase sequence of 3F6Bi during fast heating.

Analysis of the dielectric and DSC results allows the phase sequence for 3F6Bi to be determined, whilst the T_g value is taken from microscopy observations. For slow heating ($\phi \leq$ 2 K/min) the following phase transitions are observed:

GCrI ~ −90 °C CrI −18 °C SmI^*_A −6 °C CrII 20 °C SmC^*_A 112 °C SmC^* 122 °C SmA^* 130 °C Is.

(values of transition temperatures with a 1 K/min heating rate).

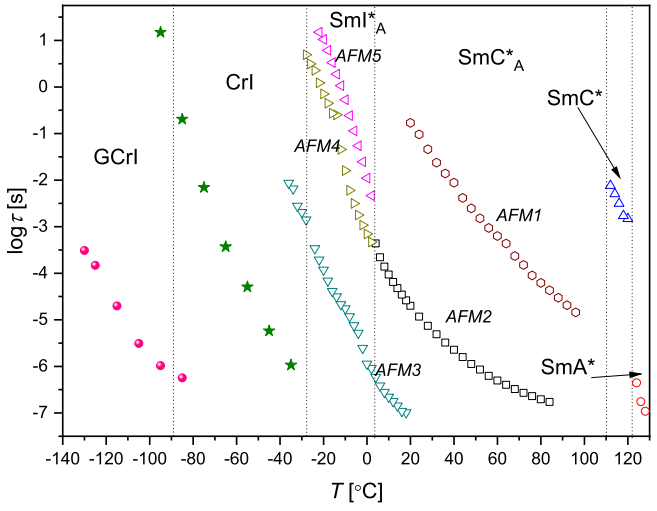

Fig. 4. The relaxation time as a function of temperature in the liquid-crystalline phases and in the CrI and GCrI, as observed during slow cooling. The vertical lines are as given by DSC thermograms and microscopic observations of the vitrification of the CrI phase.

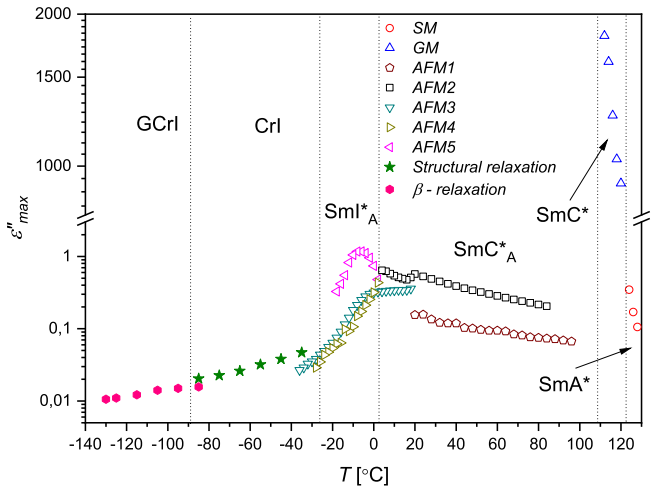

Fig. 5. The dependence of ε''_{max} as a function of temperature in the liquid-crystalline phases and in CrI and GCrI, as observed during slow cooling. The vertical lines are as in Fig. 4.

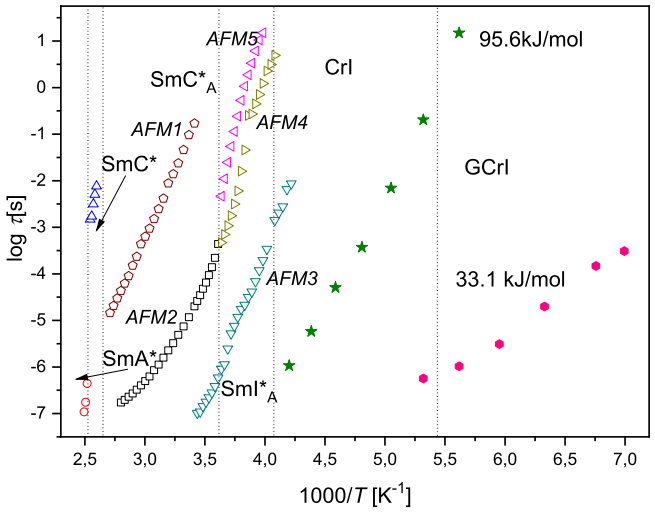

Fig. 6. Arrhenius plot of the processes observed during slow cooling in the liquid-crystalline phases and in CrI and GCrI. Vertical lines are as in Fig. 4.

For fast heating (5 K/min) the phase sequence is the following:

GCrI ~ -90 °C CrI −18 °C SmI*$_A$ 6 °C SmC*$_A$ 113 °C SmC* 123 °C SmA* 131 °C Is.

The kinetics of cold crystallization of CrII in the metastable SmI*$_A$ phase of 3F6Bi was studied systematically by DSC and dielectric spectroscopy (BDS) using non-isothermal experiments with various (0.5–2 K/min) heating rates. The degree of crystallinity, *D*, obtained from DSC experiments is defined by the following temperature function:

$$D(T) = \frac{\int_{T_o}^{T} \frac{dH}{dT} dT}{\int_{T_o}^{T_\infty} \frac{dH}{dT} dT} \quad (2)$$

where the $T_o n$ and T_∞ temperatures represent the beginning and the end of crystallization process. To calculate the temperature changes of the degree of crystallinity in BDS experiments the following formula was used:

$$D(T) = \frac{\varepsilon''(T_o) - \varepsilon''(T)}{\varepsilon''(T_o)} \quad (3)$$

where T_o is the temperature at which the value of the dielectric absorption maximum starts to decrease, and can be considered as the temperature of the beginning of the crystallization. The estimation of the degree of crystallinity in the dielectric experiment was carried out for a selected frequency of 7×10^3 Hz, characteristic for a molecular l-process in the SmI*$_A$ phase. Comparison of the degree of crystallinity changes with the temperature obtained from calorimetric (eq. (2)) and dielectric (eq. (3)) experiments is presented in Fig. 11.

It can be observed, that the beginning of the crystallization process of CrII phase depends on the heating rate, both in the calorimetric and dielectric experiments. The higher the heating rate, the higher the temperature when the crystallization begins. In the BDS method, the value of temperature corresponding to the end of crystallization ($D = 1$) is slightly dependent on the heating rate, while for the DSC method, the value of crystallization peak T_p temperature is shifted by a few °C towards higher temperatures if the heating rate increases. The parameter reflecting the influence of the heating rate on the crystallization is $T_{1/2}$, *i.e.*, the temperature at which the degree of crystallinity reaches a value of 0.5. As one can observe in this plot, $T_{1/2}$ is an increasing function of heating rate in both the DSC and BDS experiments. The differences in $T_{1/2}$ values, estimated by DSC and by BDS, grow from about 1.5 °C for 0.5 K/min to approximately 3.5 °C for 2 K/min.

Based on data shown in Fig. 11, the evolution of the crystallization over time was estimated for all heating rates. In Fig. 12, one can see that the higher the heating rate, the shorter the time of complete crystallization.

When comparing $D(t)$ results, one can see that the $t_{1/2}$ parameters obtained from DSC and BDS methods have almost the same values for both the 0.5 and 1 K/min heating rates: $t_{1/2}$–11.3 min for $\phi = 0.5$ K/min and $t_{1/2}$–6.4 min for $\phi = 1$ K/min in both methods. For heating with a 2 K/min rate, it is clearly visible that crystallization of CrII observed in the dielectric experiment goes faster than in the DSC measurements: $t_{1/2}$–3 min and 5 min in BDS and DSC methods, respectively.

The kinetics of crystallization can be considered by several models. Crystallization in the isothermal experiment can be described by the Avrami model [17,18]:

$$log - ln[1 - D(t)] = nlogt + logk \quad (4)$$

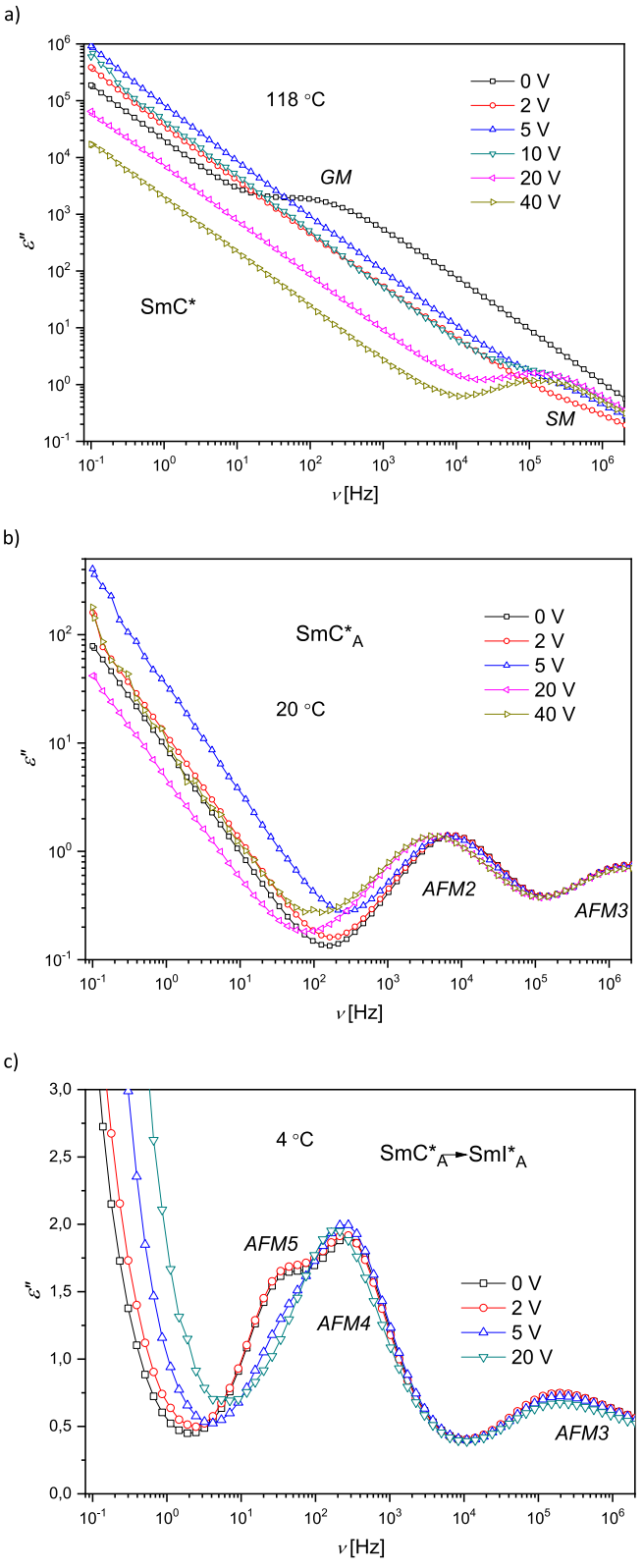

Fig. 7. Influence of the bias field on the relaxation processes in SmC*(a), SmC*$_A$ (b) and SmI*$_A$ (c) phases of 3F6Bi. The values of voltage applied to the samples of 0.07 mm thickness are given.

where $D(t)$ is a degree of crystallinity as a function of time counted from the beginning of crystallization, *n* is the parameter describing the dimensionality of the growing crystals nuclei and type of nucleation (instantaneous, prolong in time, 1-, 2- or 3-dimensional *etc.*), and the *k* parameter depends on the rate of nucleation and growth of the new crystal

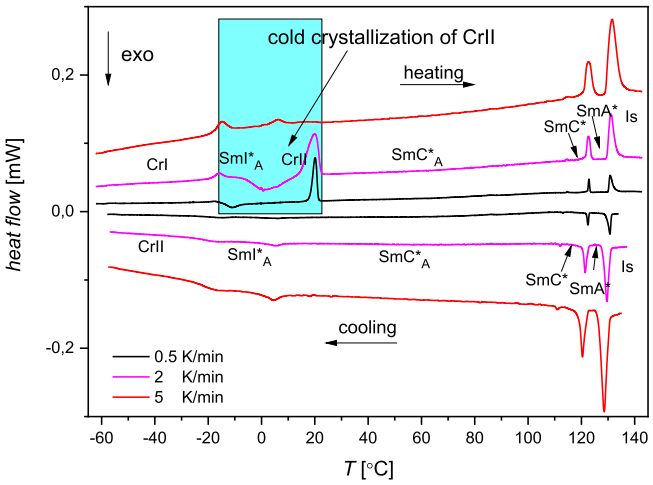

Fig. 8. The DSC thermograms of 3F6Bi recorded at selected cooling/heating rates. The marked area indicates the temperature range in which the phase sequence depends on the heating rate of the sample.

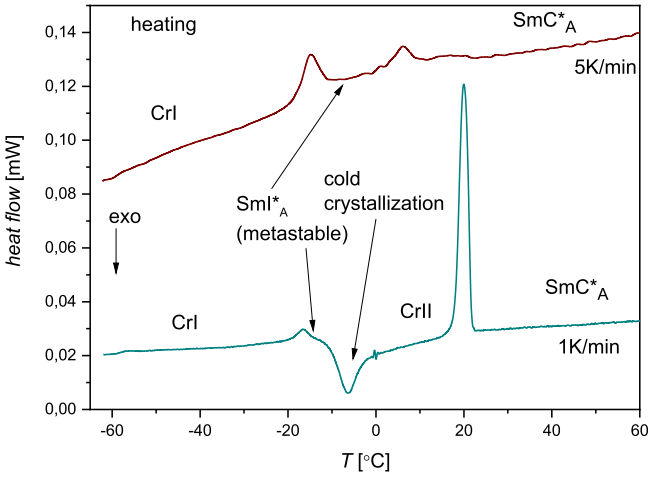

Fig. 9. The DSC curves of 3F6Bi recorded for 1 K/min and 5 K/min heating rates.

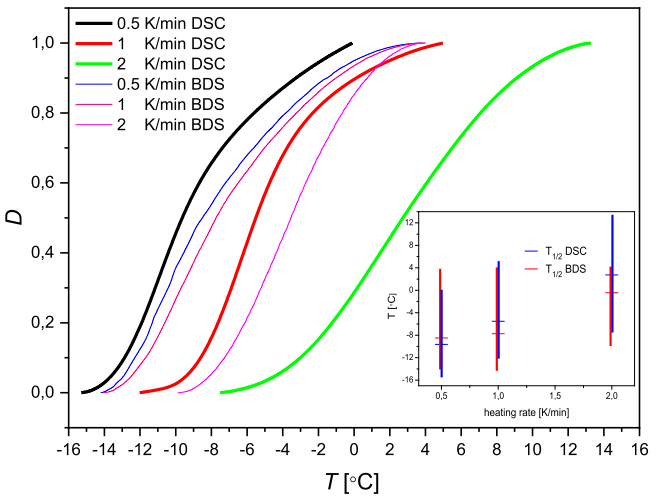

Fig. 11. Temperature dependence of the degree of crystallinity D(T) observed during cold crystallization of CrII from metastable SmI^*_A phase of 3F6Bi, for various heating rates applied in DSC and BDS experiments. The $T_{1/2}$ values estimated in both experiments are given for 0.5, 1 and 2 K/min heating rates.

phase. Modification of this equation gives the Ozawa model, which is appropriate for the description of the crystallization in non-isothermal conditions, assuming it is a process composed of many infinitesimal isothermal processes [19]:

$$log - ln[1 - D(T)] = logZ(T) - m(T)log|\phi| \quad (5)$$

with $Z(T)$ and $m(T)$ corresponding to the k and n parameters of the Avrami model, respectively. However, the Ozawa model describes crystallization in a satisfactory way when the cooling/heating rate ϕ is small. Based on these two models, Mo et al. proposed a new equation for the analysis of non-isothermal crystallization based on the equivalence of right sides of equations (5) and (6) for fixed D values [20]:

$$\log\phi = \log F(T) - a\ \log t \quad (6)$$

where a is equal to the $n\ /\ m$ ratio (n and m are exponents of the Avrami and Ozawa equations, respectively), and kinetic parameter $F(T) = [Z/k\,]^{1/m}$ is related to the cooling/heating rate. Both parameters of Eq. (6) can be estimated experimentally as a slope (a) and intercept ($\log F(T)$) of the plot of $\log\phi$ as a function of $\log t$ for a fixed value of the degree of crystallinity D of the CrII phase.

When analyze the data presented in Fig. 13 for 0.5, 1 and 2 K/min heating rates, a linear relationship $\phi(t)$ in the double logarithmic scale is observed, however the average

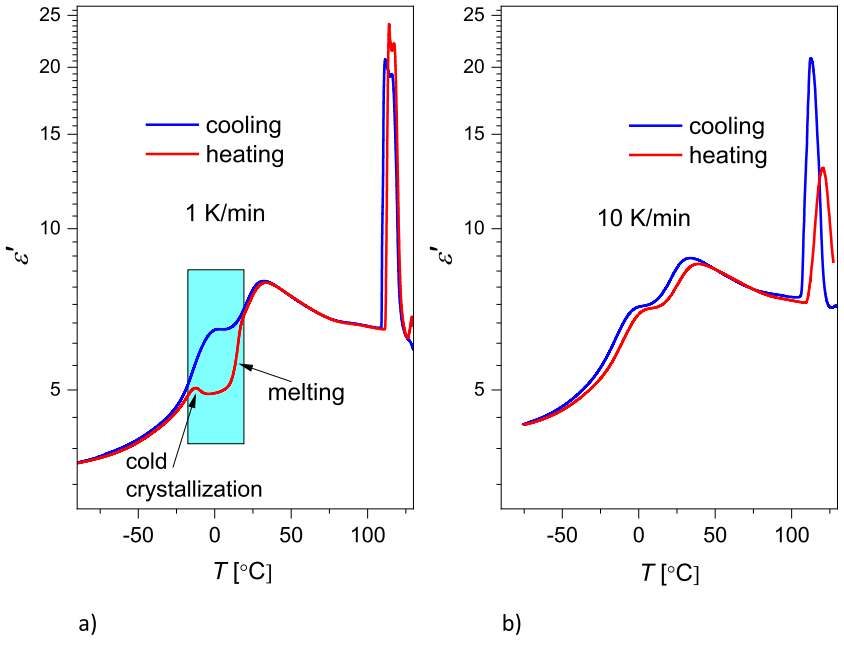

Fig. 10. The electric permittivity ε′ as a function of temperature for a selected frequency of 7 kHz, recorded during cooling and heating of 3F6Bi with 1 K/min (a) and 10 K/min (b) rates.

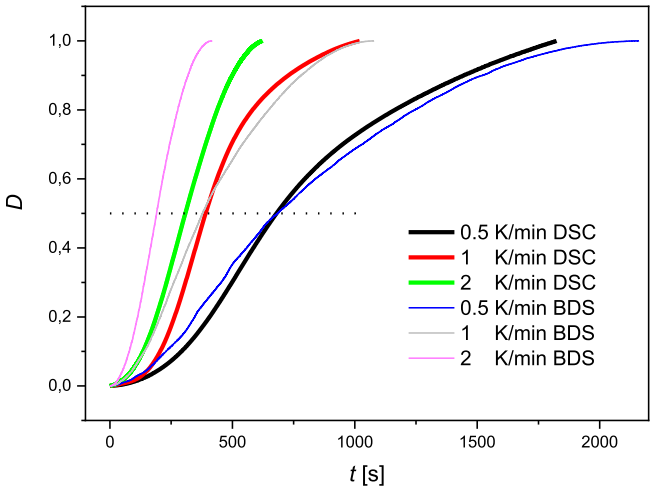

Fig. 12. The degree of crystallinity D of CrII in the metastable SmI^*_A phase of 3F6Bi for various heating rates in DSC and BDS experiments, as a function of crystallization time.

values of slopes in the BDS and DSC methods are different. The values of the calculated $log F(T)$ and $a$parameters are collated in Table 1.

As one can see in Table 1 for each of the experimental methods, raising the degree of crystallinity of CrII shows the estimated a parameter decreases systematically: from 1.80 for $D = 0.1$ to 1.27 for $D = 0.9$ (DSC) and from 1.30 for $D = 0.1$ to 0.88 for $D = 0.9$ (BDS). A slight decrease of the a parameter with the progression of crystallization process is connected with decreasing free space in a liquid limited by crystal phase growing. The parameters a describing crystal nuclei dimensionality are bigger in the case of DSC measurements than in the case of the BDS method, this results from the different features of these methods. The kinetic parameter $log F(T)$ fluctuates around the average value equal of 4.2 when estimated using the DSC results and 2.7 using BDS.

If the Kissinger model is applied to the DSC data one can estimate the activation energy E_C , which is defined as the energy needed for the transport of molecules in liquid to the surface of the growing crystal CrII phase [21]:

$$ln\frac{\phi^2}{T_P} = C - \frac{E_C}{RT_P} \tag{7}$$

where T_P is the temperature related to the DSC peak position corresponding to crystallization. Taking into account the temperature T_{on} at the beginning of the crystallization, the activation energy can be estimated using the Augis-Bennett model [22]:

$$ln\frac{\phi}{T_P - T_o n} = C_A B - \frac{E_C}{RT_P} \tag{8}$$

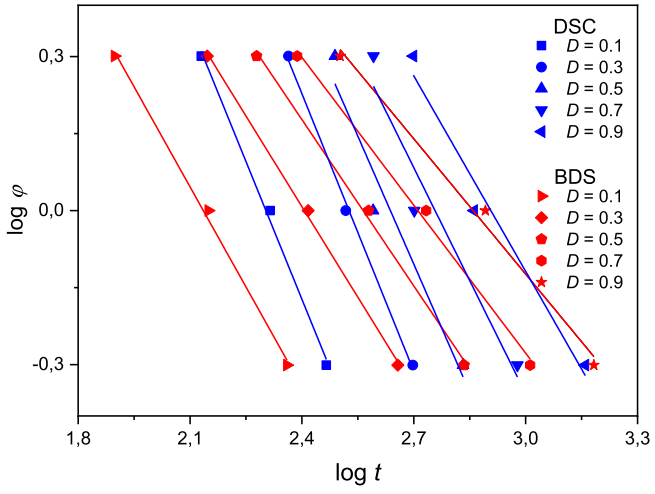

Fig. 13. Plots of $log\phi$ vs $logt$ for data obtained using DSC (blue symbols) and BDS (red symbols) experiments, for selected values of degree of crystallinity D of CrII in the SmI^*_A phase.

Table 1
The a and $log F(T)$ fitting parameters for several D values, which describe cold crystallization of the CrII phase in the metastable SmI^*_A phase of 3F6Bi, based on results of the DSC and BDS experiments.

DSC			BDS		
D	a	log(F(T))	D	a	log(F(T))
0.1	1.79	4.12	0.1	1.30	2.77
0.2	1.80	4.39	0.2	1.24	2.84
0.3	1.80	4.55	0.3	1.17	2.83
0.4	1.68	4.33	0.4	1.14	2.84
0.5	1.66	4.38	0.5	1.08	2.77
0.6	1.60	4.32	0.6	1.02	2.68
0.7	1.47	4.05	0.7	0.96	2.60
0.8	1.34	3.77	0.8	0.92	2.56
0.9	1.27	3.69	0.9	0.88	2.51

Fig. 14 shows the $ln(\phi/(T_P - T_o n))$ and $ln\left(\phi/T_P^2\right)$ plotted as a function of the inverse of the temperature. The activation energy provided with help of the Kissinger model equals 138.4 (±21,2) kJ/mol, and with help of the Augis-Bennett model it equals 99.3 (±8,0) kJ/mol. The value of the activation energy of crystallization, obtained using Eq. (8), is estimated with a smaller uncertainty than using Eq. (7), so it seems that the Augis - Bennett model is more appropriate than Kissinger model to estimate the activation energy of crystallization, for this case. A similar conclusion can be drawn for the cold crystallization of SmC^*_A [23]. The ratio of the E_c values, estimated for 3F6Bi by Eqs. (7) and (8), is typical for cold crystallization from various liquid crystal phases with a slow heating rate [6,24].

4. Conclusions

The dielectric spectra obtained over a frequency range of 3×10^{-2} to 3×10^{6} Hz and the DSC thermograms have shown a rich phase polymorphism of 4-(6-heptafluorobutanoiloxyhexyloxy)biphenyl-4′-carboxylan(S)-4-(1-methyloheptyloxy carbonyl)phenyl (3F6Bi). On cooling the isotropic liquid phase, four liquid crystal phases are observed: paraelectric (SmA*), ferroelectric (SmC*), antiferroelectric (SmC^*_A and SmI^*_A) phases, and a partially disordered CrI and its corresponding glass GCrI (identified with help of polarizing microscopy) were found and the following phase sequence deduced:

Is → SmA* → SmC* → SmC^*_A → SmI^*_A → CrI → GCrI.

The phase sequence identified on heating was the same for heating rates near 5 K/min or higher. Slight supercooling of isotropic liquid was visible. For slow heating ($\phi \leq$ 2 K/min) the following phase sequence showing cold crystallization of new CrII reveals:

GCrI → CrI → SmI^*_A → CrII → SmC^*_A → SmC* → SmA* → Is.

Studies of the crystallization kinetics of CrII in the SmI^*_A phase were performed using the DSC and BDS methods by non-isothermal experiments. To the best of our knowledge it is the first observation of cold

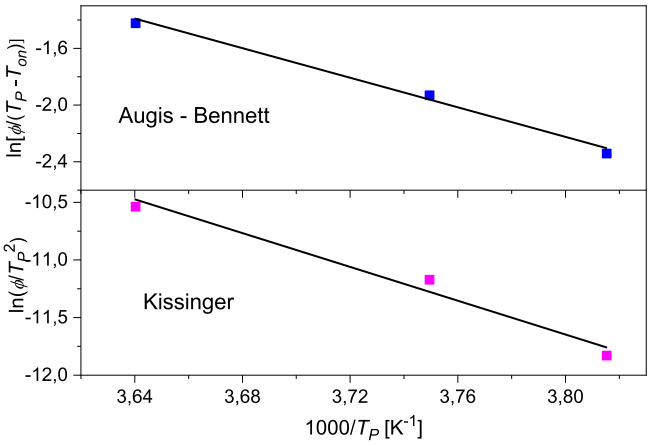

Fig. 14. Kissinger and Augis-Bennett plots for cold crystallization of the Cr II phase in the SmI^*_A of the 3F6Bi sample.

crystallization going from antiferroelectric SmI*$_A$ phase. Observations point to a higher temperature at the beginning of the crystallization process in the DSC experiment rather than in the BDS experiment. Changes to the degree of crystallinity *D* over temperature and time show the slowest process in the largest temperature range for 2 K/min, and is characterized by the highest $T_{1/2}$ value (2 °C in DSC and 0.5 °C in BDS). Using the Mo equation with a fixed *D* values, one can find that the relation between the heating rate and time of crystallization is linear over a double logarithmic scale with a negative slope. The energy needed to transport molecules in the SmI*$_A$ phase to the surface of the growing CrII nuclei was estimated, based on thermodynamic data, to be 140 kJ/mol (Kissinger model) and 100 kJ/mol (Augis-Benett model).

Dielectric spectroscopy with an applied bias field allows the identification of various types of dynamics in liquid crystalline phases. In the paraelectric SmA* and ferroelectric SmC* phases, collective relaxation processes were observed: soft mode in SmA* and Goldstone mode in SmC*. The use of a strong bias field revealed that the soft mode is also present in the SmC* phase. Three relaxation processes were observed in the antiferroelectric SmC*$_A$ and SmI*$_A$ phases. Not one of the processes in the SmC*$_A$ phase is sensitive to the bias field, so two of them have been identified as molecular processes, *i.e.* the s-process (the slowest) and the l-process (the fastest) related to the reorientation of the molecules around the short and long axes, respectively. The third of these processes is probably a collective ferroelectric amplitudon, surviving the SmC*$_A$ – SmI*$_A$ transition similarly as l-process. The third process in SmI*$_A$ corresponds to ferroelectric phason and is the slowest one. In the partially disordered CrI phase a weak non-Debye relaxation was registered which may be ascribed to intramolecular motions of the terminal chains, strongly correlated in local and long-range scales. In the GCrI phase these motions are frozen-in and a secondary β-relaxation with an Arrhenius character was detected.

References

[1] J. Herman, P. Harmata, O. Strzeżysz, M. Czerwiński, S. Urban, P. Kula, Synthesis and properties of chosen 4-butyl-phenyltolane derivatives – on the influence of core substitution on birefringence, mesomorphic and dielectric properties, J. Mol. Liq. 267 (2018) 511–519.

[2] J. Hoffmann, K. Nowicka, W. Kuczyński, N. Bielejewska, Experimental evidence of soft mode in the smectic C*$_\alpha$ phase of chiral ferroelectric liquid crystals, Soft Mater. 10 (2014) 8548–8557, https://doi.org/10.1039/C4SM01631A.

[3] H. Takezoe, E. Górecka, M. Čepič, Antiferroelectric liquid crystals: interplay of simplicity and complexity, Rev. Mod. Phys. 82 (2010) 897–937, https://doi.org/10.1103/RevModPhys.82.897.

[4] T. Rozwadowski, M. Massalska-Arodź, M. Jasiurkowska-Delaporte, Negative pressure effects on molecular dynamics and phase diagram of glass-forming nematic liquid crystal 4-cyano-3-fluorophenyl 4-butylbenzoate (4CFPB) confined in nanopores, J. Mol. Liq. 279 (2019) 127–132, https://doi.org/10.1016/j.molliq.2019.01.106.

[5] M. Jasiurkowska-Delaporte, S. Napolitano, J. Ley, E. Juszyńska-Gałązka, M. Wubbenhorst, M. Massalska-Arodź, Glass transitions dynamics and crystallization kinetics in the smectic liquid crystal 4-n-buyloxybenzylidene-4'-n'-octylaniline (BBOA), J. Phys. Chem. B 120 (2016) 12160–12167.

[6] T. Rozwadowski, M. Massalska-Arodź, Ł. Kolek, K. Grzybowska, A. Bąk, K. Chłędowska, Kinetics of cold crystallization of 4-Cyano-3-fluorophenyl4-Butylbenzoate (4CFPB) glass forming liquid crystal.I. Nonisothermal process as studied by microscopic, calorimetric, and dielectric methods, Cryst. Growth Des. 15 (2015) 2891–2900, https://doi.org/10.1021/acs.cgd.5b00328.

[7] Ł. Kolek, M. Massalska-Arodź, D. Majda, B. Wantusiak, S. Zalewski, P. Kula, Studies of phase diagram of a liquid crystal with 4-[2-(3-Fluorophenyl)ethyl]biphenyl core of molecules, Acta Phys. Pol. 122 (2012) 370–374.

[8] R. Dąbrowski, P. Kula, Z. Raszewski, W. Piecek, J.M. Otón, A. Spadło, New orthoconic antiferroelectrics useful for applications, Ferroelectrics 395 (2010) 116–132.

[9] R. Dąbrowski, W. Drzewiński, J. Dziaduszek, J. Gąsowska, P.A. Henderson, P. Kula, J.M. Otón, N. Bennis, Orthonic antiferroelectric liquid crystals containing biphenyl, terphenyl, or naphthyl mesogenic unit, Opto-Electron. Rev. 15 (1) (2007) 32–36.

[10] M. Jasiurkowska-Delaporte, E. Juszyńska, Ł. Kolek, J. Krawczyk, M. Massalska-Arodź, N. Osiecka, T. Rozwadowski, Signatures of glass transition in partially ordered phases, Liq. Cryst. 40 (2013) 1436–1442.

[11] Ł. Kolek, M. Massalska-Arodź, D. Majda, B. Suchodolska, S. Zalewski, Studies of phase diagram and glass transition of a liquid crystal with ferro- and antiferroelectric phases, Acta Phys. Pol. 124 (2013) 909–912.

[12] Y. Uchiyama, H. Moritake, M. Ozaki, K. Yoshino, H. Taniguchi, K. Satoh, T. Tani, K. Fujisawa, Dielectric properties in ferroelectric and antiferroelectric liquid crystals with isotropic-chiral smectic C phase sequence, Jpn. J. Appl. Phys. 32 (1993) 4335.

[13] S. Hiller, S. Pikin, W. Haase, J. Goodby, I. Nishiyama, Relaxation processes in the antiferroelectric phase as studied by dielectric spectroscopy, Jpn. J. Appl. Phys. 33 (1994) L1170.

[14] M. Buivydas, F. Gouda, G. Andersson, S. Lagerwall, B. Stebler, J. Bomelburg, G. Heppke, B. Gestblom, Collective and non-collective excitations in antiferroelectric and ferrielectric liquid crystals studied by dielectric relaxation spectroscopy and electro-optic measurements, Liq. Cryst. 23 (1997) 723–739.

[15] Yu P. Panarin, O. Kalinovskaya, J.K. Vij, The investigation of the relaxation processes in antiferroelectric liquid crystals by broad band dielectric and electro-optic spectroscopy, Liq. Cryst. 25 (1998) 241–252.

[16] Ł. Kolek, M. Massalska-Arodź, M. Paluch, K. Adrjanowicz, T. Rozwadowski, D. Majda, Dynamics in ferro- and antiferroelectric phases of a liquid crystal with fluorinated molecules as studied by dielectric spectroscopy, Liq. Cryst. 40 (2013) 1082–1088.

[17] M. Avrami, Kinetics of phase change. I. General Theory, J. Chem. Phys. 7 (1939) 1103–1112.

[18] M. Avrami, Kinetics of phase change. II. Transformation−time relations for random distribution of nuclei, J. Chem. Phys. 8 (1940) 212–224.

[19] T. Ozawa, Kinetics of non-isothermal crystallization, Polymer 12 (1971) 150–158.

[20] Y. An, L. Dong, Z. Mo, T. Liu, Z. Feng, Nonisothermal crystallization kinetics of poly(β-hydroxybutyrate), J. Polym. Sci. 36 (1998) 1305–1312.

[21] H.E. Kissinger, Variation of peak temperature with heating rate in differential thermal analysis, J. Res. Natl. Bur. Stand. 57 (1956) 217–221.

[22] J.A. Augis, J.E. Bennett, Calculation of the Avrami parameters for heterogeneous solid state reactions using a modified Kissinger model, J. Therm. Anal. 13 (1978) 283–292.

[23] A. Deptuch, T. Jaworska-Gołąb, M. Marzec, M. Urbańska, M. Tykarska, Cold crystallization from chiral smectic phase, Phase Transitions 92 (2) (2019) 126–134.

[24] M. Jasiurkowska-Delaporte, T. Rozwadowski, E. Juszynska-Gałązka, J. Krawczyk, E. Dmochowska, P. Kula, M. Massalska-Arodź, Relaxation dynamics and crystallization study of glass-forming chiral-nematic liquid crystal S,S-2,7-bis(4-pentylphenyl)-9,9dimethylbutyl 9H-fluorene (5P-Am∗FLAm∗-P5), Eur. Phys. J. E. 42 (2019) 121.